

## Numerical Investigation of Compressive Strength of Structural Steel Material Under Different Loads According to ASTM D695 Standard

Muhammed Safa KAMER<sup>1,a</sup>

<sup>1</sup>Kahramanmaraş Sutcu Imam University, Faculty of Engineering and Architecture, Department of Mechanical Engineering, Kahramanmaraş, Türkiye

<sup>a</sup>ORCID: 0000-0003-3852-1031

### Article Info

Received : 01.01.2025

Accepted : 25.03.2025

DOI: 10.21605/cukurovaumfd.1666074

### Corresponding Author

Muhammed Safa KAMER  
msafakamer@ksu.edu.tr

### Keywords

Ansys

ASTM D695

Compressive strength test

Explicit dynamics

Numerical analysis

**How to cite:** KAMER, M.S., (2025). Numerical Investigation of Compressive Strength of Structural Steel Material Under Different Loads According to ASTM D695 Standard. Çukurova University, Journal of the Faculty of Engineering, 40(1), 227-237.

### ABSTRACT

In order to determine the mechanical properties of materials according to certain standards, numerical analysis methods are frequently used in addition to experimental studies. In this study, the compressive strength test was numerically modeled in a computer environment according to the ASTM D695-15 standard. Analyses were carried out by defining structural steel material for the plate designed with the specified standard dimensions and 1 mm thickness. In the numerical analysis, two different loading types, force and displacement, were examined. Numerical analyzes were carried out in a total of twelve different situations by applying 2, 4, 6, 8, 10 and 12 N compressive forces in the analyzes where force load (FL) was applied, and 1, 2, 3, 4, 5 and 6 mm compressive displacements in the analyzes where displacement load (DL) was applied. The effects of different loading types and different loading intensities on the compressive strength of the test specimen were investigated. In all analyses where FL and DL were defined, it was determined that as the FL and DL intensity increased, the stresses and total deformation on the test specimen also increased.

## Yapısal Çelik Malzemenin Farklı Yükler Altındaki Basınç Dayanımının ASTM D695 Standardına Göre Sayısal Olarak İncelenmesi

### Makale Bilgileri

Geliş : 01.01.2025

Kabul : 25.03.2025

DOI: 10.21605/cukurovaumfd.1666074

### Sorumlu Yazar

Muhammed Safa KAMER  
msafakamer@ksu.edu.tr

### Anahtar Kelimeler

Ansys

ASTM D695

Basınç dayanımı testi

Explicit dynamics

Sayısal analiz

**Atf şekli:** KAMER, M.S., (2025). Yapısal Çelik Malzemenin Farklı Yükler Altındaki Basınç Dayanımının ASTM D695 Standardına Göre Sayısal Olarak İncelenmesi. Çukurova Üniversitesi, Mühendislik Fakültesi Dergisi, 40(1), 227-237.

### ÖZ

Malzemelerin belirli standartlara göre mekanik özelliklerinin belirlenmesi amacıyla deneysel çalışmaların yanında sayısal analiz yöntemleri de sıklıkla kullanılmaktadır. Bu çalışmada, basınç dayanımı testi ASTM D695-15 standardına göre bilgisayar ortamında sayısal olarak modellenmiştir. Belirtilen standart ölçülerinde ve 1 mm kalınlığında tasarlanan levhaya yapısal çelik malzeme tanımlanarak analizler gerçekleştirilmiştir. Sayısal analizlerde kuvvet ve deplasman olmak üzere iki farklı yükleme tipi incelenmiştir. Kuvvet yükü (FL) uygulanan analizlerde 2, 4, 6, 8, 10 ve 12 N basma kuvvetlerinin, deplasman yükü (DL) uygulanan analizlerde ise 1, 2, 3, 4, 5 ve 6 mm basma deplasmanlarının uygulanmasıyla toplam oniki farklı durumda sayısal analizler gerçekleştirilmiştir. Farklı yükleme tipi ve farklı yükleme şiddetlerinin test numunesinin basınç dayanımı üzerindeki etkileri araştırılmıştır. FL ve DL tanımlanan tüm analizlerde FL ve DL şiddetinin artmasıyla, test numunesi üzerindeki gerilmelerin ve toplam deformasyonun da arttığı belirlenmiştir.

## 1. INTRODUCTION

In recent years, software that works with the finite element method is frequently used to evaluate the mechanical properties of materials and determine the behavior of machine components under various loads. One of the most commonly used software for determining the mechanical behavior of materials through the finite element method is Ansys. The Ansys software contains many modules, and some of the modules used for determining mechanical behaviors include Composite PrePost, Explicit Dynamics, and Static Structural. By using these modules, numerical analyses can be conducted by defining the loads acting on machine components, or by modeling the relevant test standards to determine the mechanical behaviors of materials through numerical analysis. The literature contains many standards for determining the mechanical properties of materials, one of which is the ASTM D695 compression strength test standard. This standard involves testing specimens with specific cross-sectional profiles (circular section, square section) to determine the compression strength of materials, as well as testing plates of the specified dimensions (Figure 2) using the relevant test equipment (Figure 1). Numerous studies have been conducted in the literature using both of these methods separately for compression strength testing.

In the literature, many studies have been conducted using test specimens with specific cross-sectional profiles for compression strength testing, some of which are provided here. Dwivedi et al. [1] investigated the parameters affecting the mechanical properties of 3D printed PLA+ diamond lattice structures. They tested the effects of various factors on compressive strength and energy absorption. Additionally, by using nature-inspired machine learning algorithms, they improved the accuracy of model predictions. As a result, they identified cell size as an important factor for compressive strength. Vidakis et al. [2] investigated the effects of seven control parameters on the energy consumption and mechanical properties of PLA samples produced with a 3D printer. In the experiments, they tested parameters such as energy consumption, production time, and compressive strength. They found that printing speed and layer thickness are the most significant factors affecting energy consumption, while infill density and orientation angle have an impact on compressive strength. Claudio et al. [3] investigated the behavior of PLA material under compression. They experimentally determined the effects of printing parameters on the compressive behavior of PLA samples. They found that compressive strength is directly proportional to density, while no such relationship was found for fatigue. Johri et al. [4] performed finite element modeling of natural fiber-reinforced polymeric hybrid composites. They modeled jute fabric using Texgen and calculated the elastic constants. They found that the mechanical properties they calculated showed a low deviation when compared to experimental data. As a result, they concluded that chicken feather fiber reduces density, while jute fiber enhances mechanical durability. Pernet et al. [5] examined the mechanical behavior and the economic and environmental benefits of different infill patterns. Through compressive tests using 14 different infill patterns, they analyzed the relationships between load and weight. In their study, they provided comprehensive information on mechanical properties for product design and manufacturing. Additionally, the study identified opportunities for more robust infill pattern designs for additive manufacturing. Selvamani et al. [6] investigated the bending and compressive properties of rice-reinforced PLA composites. They conducted bending and compression tests according to ASTM standards and analyzed the effects of different infill patterns and compositions using response surface methodology. As a result, they found that a 15 wt% rice content provided better properties, while a 70 wt% rice content created lower interlayer adhesion energy. Additionally, they identified concentric and grid patterns as the best printing patterns for bending and compression properties. Subramaniyan et al. [7] investigated the use of PLA and its composites for producing sandwich structures. They focused on the environmental friendliness of PLA and its performance. They explored the compressive properties of 3D printed sandwich structures and methods to improve the mechanical properties. Srinivasan et al. [8] studied the effects of hygrothermal aging on the performance of glass fiber reinforced IPN composites. They aged samples containing polyurethane and vinyl ester by exposing them to water at different temperatures. The tests showed that temperature and aging time slightly reduced the strength of the GFRP tubes. Additionally, they found that as the proportion of PU prepolymer increased, the geometric structure of the samples was maintained. Morales et al. [9] investigated the effect of interlayer waiting times on the mechanical properties of ABS structures produced by 3D printing. They found that increasing the waiting time between layers led to a reduction in both compressive and shear strength. The study concluded that greater care should be taken when selecting print settings, as printing processes requiring additional time could negatively affect the mechanical strength. Vidakis et al. [10] examined the compressive strength of ABS and ABS plus parts produced with different manufacturing parameters. They experimentally revealed the durability differences

between ABS and ABS plus. They found that ABS parts produced with a larger layer thickness showed lower compressive strength, while ABS plus parts exhibited higher durability.

In the literature, many studies have been conducted where plates of the dimensions specified in the relevant standard are tested using the appropriate testing apparatus for compressive strength tests, and some of these studies are presented here. Cocchi et al. [11] used flat hourglass-shaped specimens to evaluate the compressive behavior of FRP. The hourglass shape reduces stress concentration by ensuring damage occurs at the center. They assessed the specimens using four-point bending and ASTM D695 compression tests on E-glass/epoxy and carbon/PEEK composite materials. Haseebuddin et al. [12] examined the mechanical properties of polyester composites reinforced with different percentages of PET flakes. They found that as the PET flake percentage increased up to 15%, the hardness increased, the composite with 10 % PET flakes exhibited the maximum tensile strength, and the composite with 5 % PET flakes showed the maximum compressive strength. They studied the fracture morphology using scanning electron microscopy. As a result, they demonstrated that the PET flake percentages had a significant impact on the mechanical properties. Squires et al. [13] investigated the compressive strength of unidirectional carbon fiber by examining preparation and configuration variables. They measured compressive strength using the ASTM D 695 M test method and conducted damage evaluations using SEM microscopy. The results showed that the quality of specimen preparation was a significant factor influencing the damage mechanism. They demonstrated that the preparation quality directly affected the compressive strength.

In this study, the compressive strength test was numerically modeled in a computer environment according to the ASTM D695-15 standard. Numerical analyses were carried out in the “Explicit Dynamics” module of the Ansys Workbench R19.2 program. Structural steel material was defined for the plate designed with standard dimensions (Figure 2) and 1 mm thickness, and the analyses were performed. Two different loading types, force and displacement, were examined in the numerical analyses. In the FL applied analyses, six different compressive forces (2 N, 4 N, 6 N, 8 N, 10 N, and 12 N) and in the DL applied analyses, six different compressive displacements (1 mm, 2 mm, 3 mm, 4 mm, 5 mm, and 6 mm) were applied, resulting in a total of twelve different cases for the numerical analyses. The effects of different loading types and loading intensities on the compressive strength of the test specimens were investigated. As it is known, ASTM D695-15 standard is defined for rigid plastic materials. In this study, instead of plastic material, Structural steel material was selected from the Ansys Workbench R19.2 program “Explicit Materials” library, which can be easily found in the market, to perform the test when necessary. The aim of this study is to determine the necessary parameters for the numerical analysis of the compression test in the Ansys Workbench R19.2 program in accordance with the ASTM D695-15 standard. Our next study will be to supply the necessary apparatus and perform the tests for the application of the ASTM D695-15 standard in the compression test device. In this way, the verification of the experimental and numerical studies can be done. Afterwards, it is planned to perform the tests and numerical analyzes of plastic and composite materials according to the ASTM D695-15 standard using the obtained data and determined parameters.

## 2. MATERIALS AND METHOD

The ASTM D695-15 [14] compressive strength test rig generally consists of support jigs, the test specimen, and the heads of the compressive test machine (Figure 1).

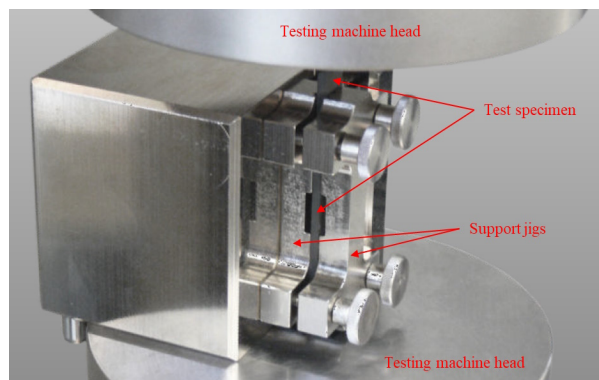


Figure 1. ASTM D695 compressive strength test rig [15]

In order to perform numerical analyses, firstly, the solid model designs of the schematic support jig created using the surfaces of the test specimen and support jigs in contact with the test specimen were performed in the SolidWorks 2018 program (Figure 2). Assembly designs consisting of the test specimen and schematic support jigs were made. Only the parts of the support jigs shown in Figure 1 that are in contact with the test specimen were designed to be used in analyses, and each surface of these elements was given a thickness of 0.4 mm. As seen in Figure 2, at the beginning of the test, there was a test distance of 6.4 mm between the upper surface of the test specimen and the upper surface of the schematic support jig.

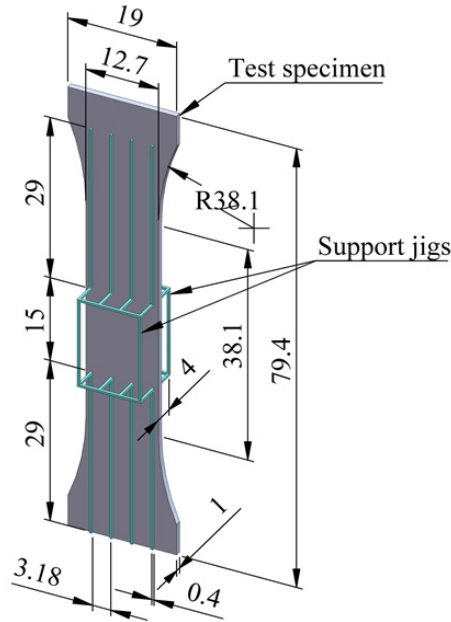


Figure 2. Solid model used in numerical analysis

The designed solid model (Figure 2) was transferred to the “Explicit Dynamics” module in the Ansys Workbench R19.2 program. Structural steel material definition was made for all elements in the analysis design. The structural steel material properties used in the analysis were given in Table 1. Afterwards, frictionless contact relations were defined between the front and back surfaces of the test specimen and the relevant surfaces where the support jigs was in contact. In this way, the test specimen was able to move between the support jigs when necessary under the effect of the compression load.

Table 1. Structural steel material properties

Density	7.85 g/cm <sup>3</sup>
Young's modulus	200 GPa
Tensile yield strength	250 MPa
Tensile ultimate strength	460 MPa

The mesh properties used in the numerical analyses were given in Table 1. The mesh image of the test specimen and support jigs created using the properties specified in Table 1 was shown in Figure 3 together with the detailed image.

Table 2. Mesh properties

Body sizing - Element size - Test specimen	1 mm
Body sizing - Element size - Support jigs	0.4 mm
Hex dominant method - Support jigs	All quad
Max. Skewness	0.25244
Min. Orthogonal Quality	0.925
Number of nodes	9664
Number of elements	3153

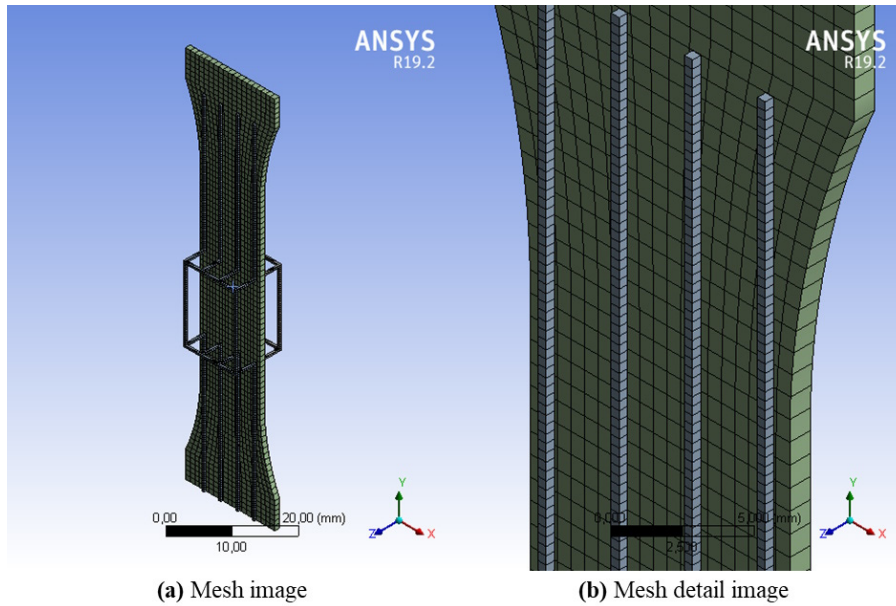


Figure 3. Mesh images

In the numerical analysis, all surfaces of the schematic support jigs and the bottom surface of the test specimen were selected and the fixed support boundary condition was defined (Figure 4). In the numerical analyses applied to FL, force and displacement boundary conditions were defined on the upper surface of the test specimen (Figure 4a). In the displacement boundary condition, the upper surface of the test specimen was fixed (0 mm) in the X and Z axes and left free in the Y axis. In the force boundary condition, no force (0 N) was defined on the upper surface of the test specimen in the X and Z axes, and six different numerical analysis were performed by applying compressive forces of 2 N, 4 N, 6 N, 8 N, 10 N and 12 N in the negative direction in the Y axis. In the numerical analyses applied to DL, a displacement boundary condition was defined on the upper surface of the test specimen (Figure 4b). In the displacement boundary condition, the upper surface of the test specimen was fixed (0 mm) in the X and Z axes, and six different numerical analysis were performed by applying compressive displacements of 1 mm, 2 mm, 3 mm, 4 mm, 5 mm and 6 mm in the negative direction in the Y axis. All numerical analyses were performed using a end time of 0.02 s. As a result of numerical analysis, the stress and deformation behaviors of the test specimen under compressive loads at different forces and different displacements were investigated.

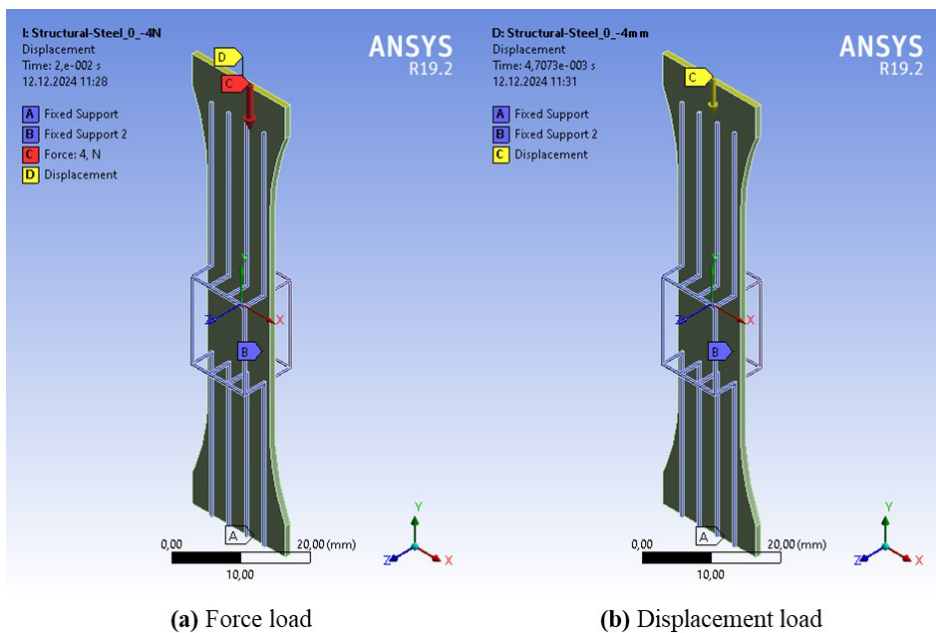


Figure 4. Boundary conditions images used in numerical analysis

### 3. RESULTS AND DISCUSSION

Equivalent Von Mises stress contour images obtained from numerical analyses performed under different compressive forces by defining FL were shown in Figure 5. When the figure was examined, it was seen that the stresses on the test specimen increase as the applied force increases. It was determined that the test specimen did not suffer buckling damage in the analyses performed with 2 N, 4 N and 6 N compression forces, some buckling occurred in the analyses performed with 8 N and 10 N compression forces, and the test specimen was completely deformed in the analyses performed with 12 N compression force. In the analyses where buckling occurs, it was seen that the buckling occurs in the middle region of the test specimen. There is some opening in the middle regions of the support jigs used in the compressive strength test, and the test mechanism ensures that buckling occurs in this region.

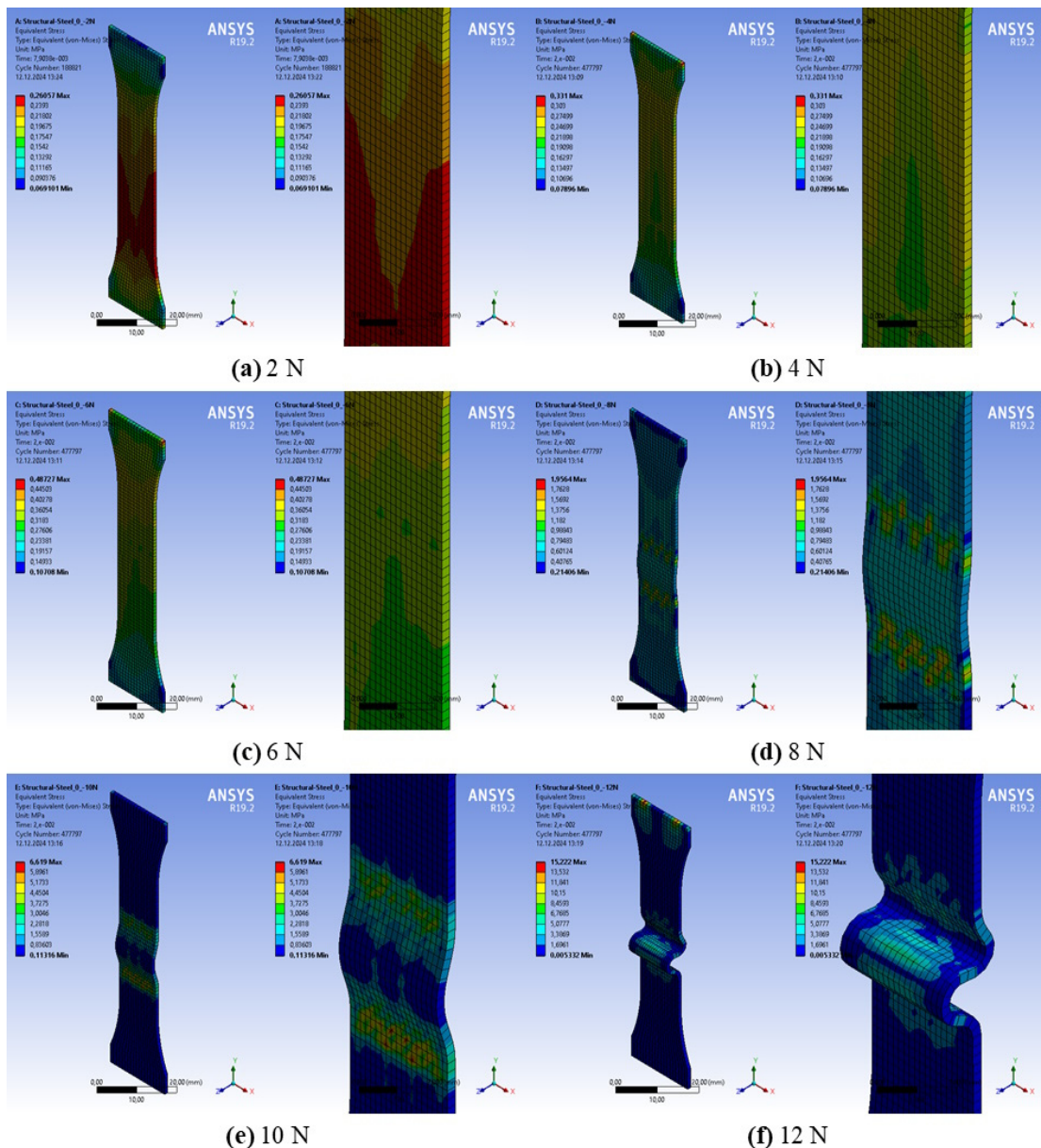


Figure 5. Equivalent stress images obtained from numerical analysis where force load is defined

Total deformation contour images obtained from numerical analyses performed under different compression forces by defining FL were shown in Figure 6. When the figure was examined, it was seen that the total deformation on the test specimen increases with the increase in the applied force. In the

analysis performed with 4 N compression force, it was observed that some compression deformation begins in the middle region of the test specimen, in the analysis performed with 6 N compression force, the compression deformation in the middle region spreads to the entire section, and in the analysis performed with 8 N compression force, buckling begins in the middle region. In the analyses performed with 8 N and 10 N compressive forces, it was determined that the highest total deformation occurred in the middle regions of the test specimen, and in the analyses performed with 12 N compressive force, the highest total deformation occurred in the upper part of the test specimen. In fact, it is not expected that a force of 12 N would cause such a deformation in the structural steel material in the specified cross-sectional area. It can be said that this deformation damage occurred due to reasons such as the low thickness of the compression test specimen, the material being forced to buckle rather than to compress due to the gap in the middle area of the test apparatus, and the formation of a high-speed impact effect in the analysis as a result of the analysis time of 0.02 s determined in the boundary conditions of the maximum deformation occurring in the analysis.

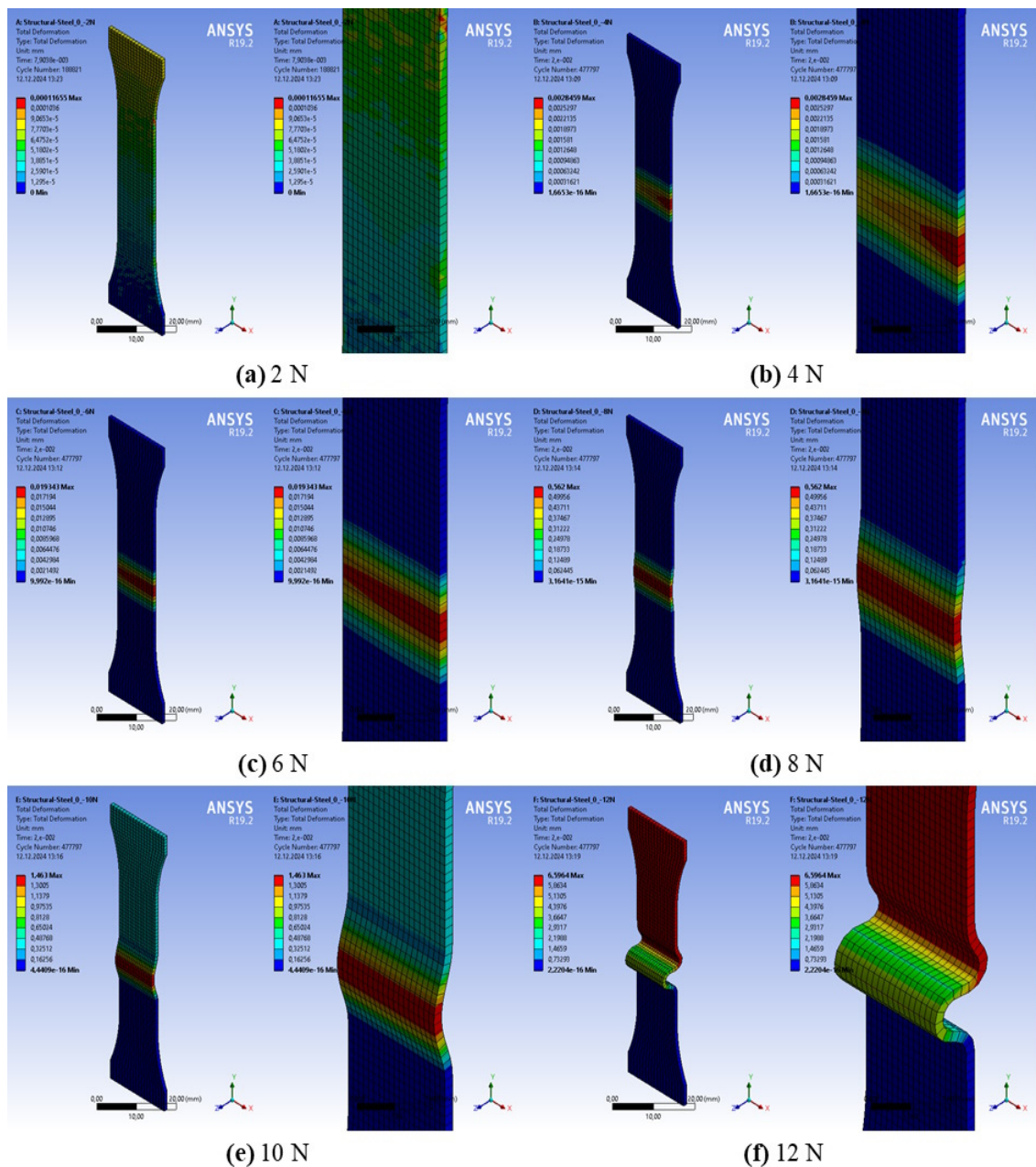


Figure 6. Total deformation images obtained from numerical analysis where force load is defined

Equivalent Von Mises stress contour images obtained from numerical analyses performed under different compressive displacements by defining DL were shown in Figure 7. When the figure was examined, it was seen that the stresses on the test specimen increase with the increase in the applied displacement. It was determined that buckling damage occurred in all of the different compression displacements applied, that the amount of buckling increased as the amount of displacement increased, and that the buckling occurred in the middle regions of the test specimen.

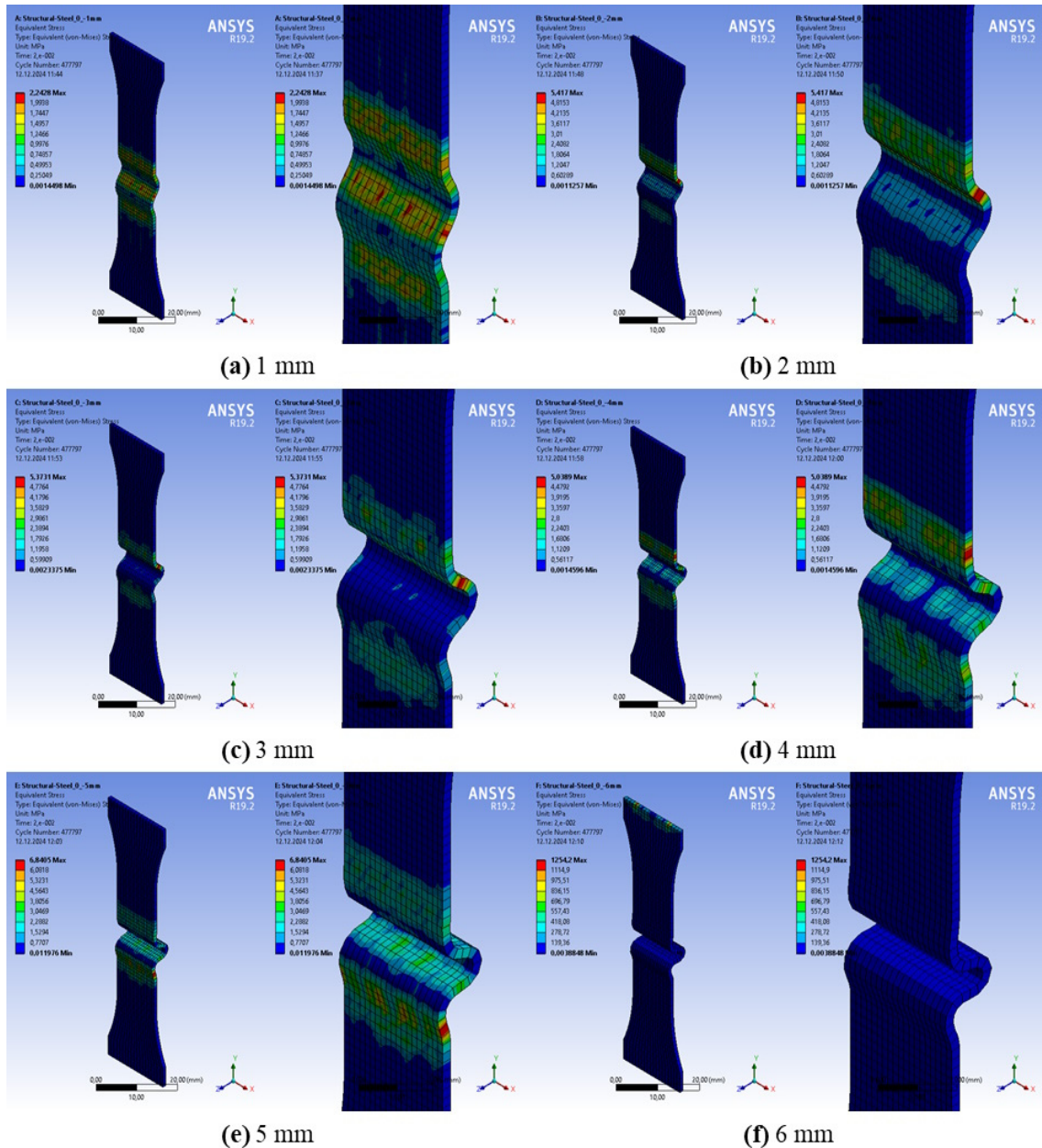
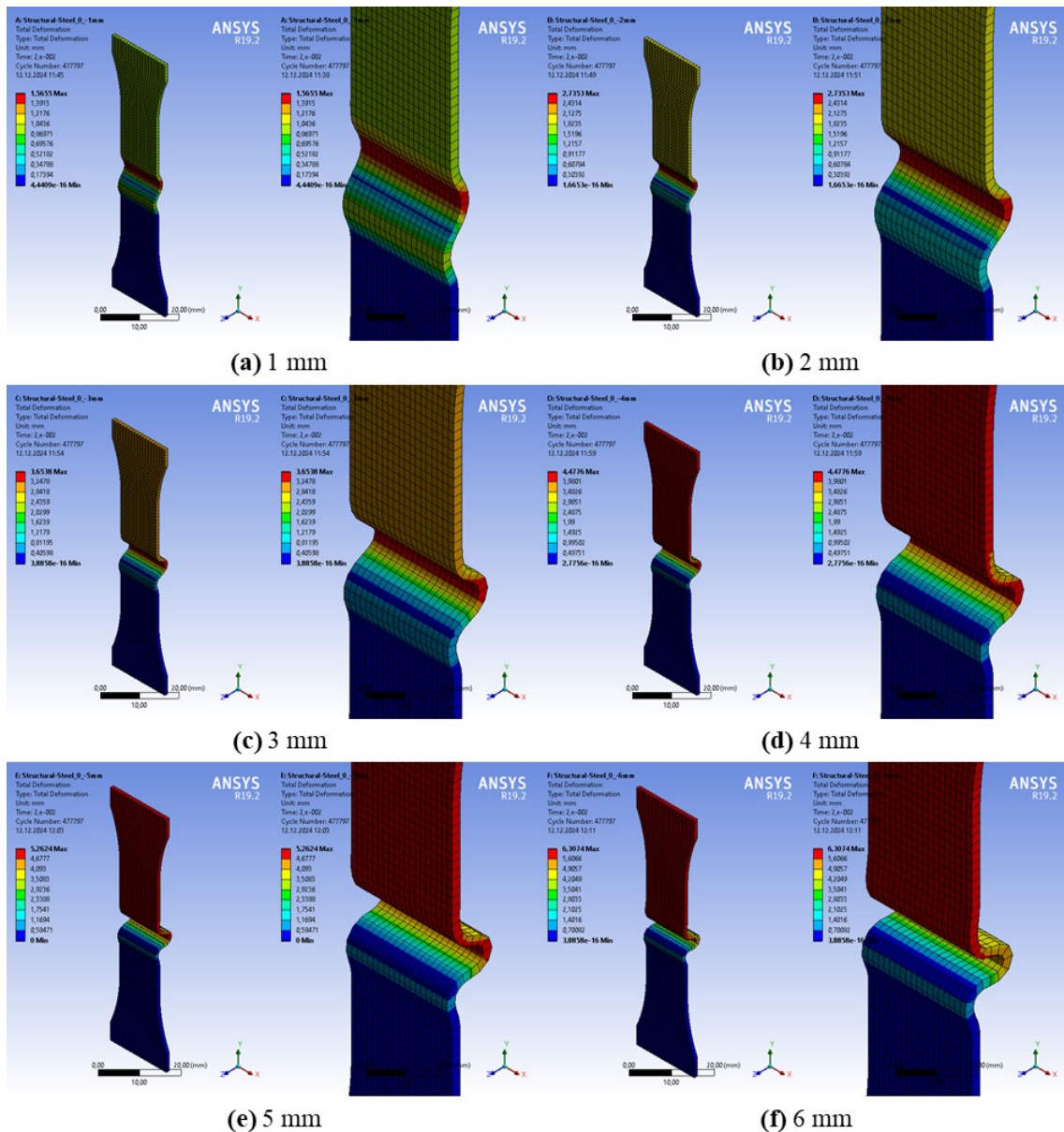


Figure 7. Equivalent stress images obtained from numerical analysis where displacement load is defined

Total deformation contour images obtained from the numerical analyses performed under different compression displacements by defining DL were shown in Figure 8. When the figure was examined, it was seen that the total deformation on the test specimen increases with the increase in the applied displacement. In the analyses performed with 1 mm, 2 mm and 3 mm compression displacements, it was determined that the highest total deformation occurred in the middle regions of the test specimen, and in the analyses performed with 4 mm, 5 mm and 6 mm compression displacements, it was determined that the highest total deformation occurred in the upper part of the test specimen.



**Figure 8.** Total deformation images obtained from numerical analysis where displacement load is defined

The result graphs obtained from the numerical analysis performed by defining FL and DL were shown in Figure 9. When the maximum equivalent stress (MES) – time graph obtained from the numerical analysis performed by defining FL was examined (Figure 9a), it was determined that the MES values of the test specimens increased with the increase in the applied compressive force, and that the test specimens exhibited creep behavior at this value for a while after reaching certain MES values. It was observed that in the analyses performed with 2 N, 4 N and 6 N compressive forces, the analyses were terminated after the test specimen has crept to some extent, and in the analyses performed with 8 N, 10 N and 12 N compressive forces, the analyses were terminated with the rapid increase in the MES values after the test specimen has crept to some extent. When the maximum total deformation (MTD) – time graph obtained from the numerical analysis performed by defining FL was examined (Figure 9b), it was determined that the MTD values of the test specimens increased with the increase in the applied compression force. In the analyses performed with all compression forces, it was observed that the increase in the MTD values of the test specimens initially remained low for a while, and then the increase in the MTD values gradually reached higher values. When the MES – time graph obtained from the numerical analysis performed by defining DL was examined (Figure 9c), it was seen that the MES values of the test specimens increase with the increase in the applied compression displacement, yielding occurs after the test specimens reach certain

MES values, and the test specimens undergo plastic deformation after this region. When the MTD – time graph obtained from the numerical analysis performed by defining DL was examined (Figure 9d), it was determined that the MTD values of the test specimens increased with the increase in the applied compressive displacement. It can be said that in the analyses performed with all compression displacements, the MTD values of the test specimens increased with a somewhat linear behavior depending on time.

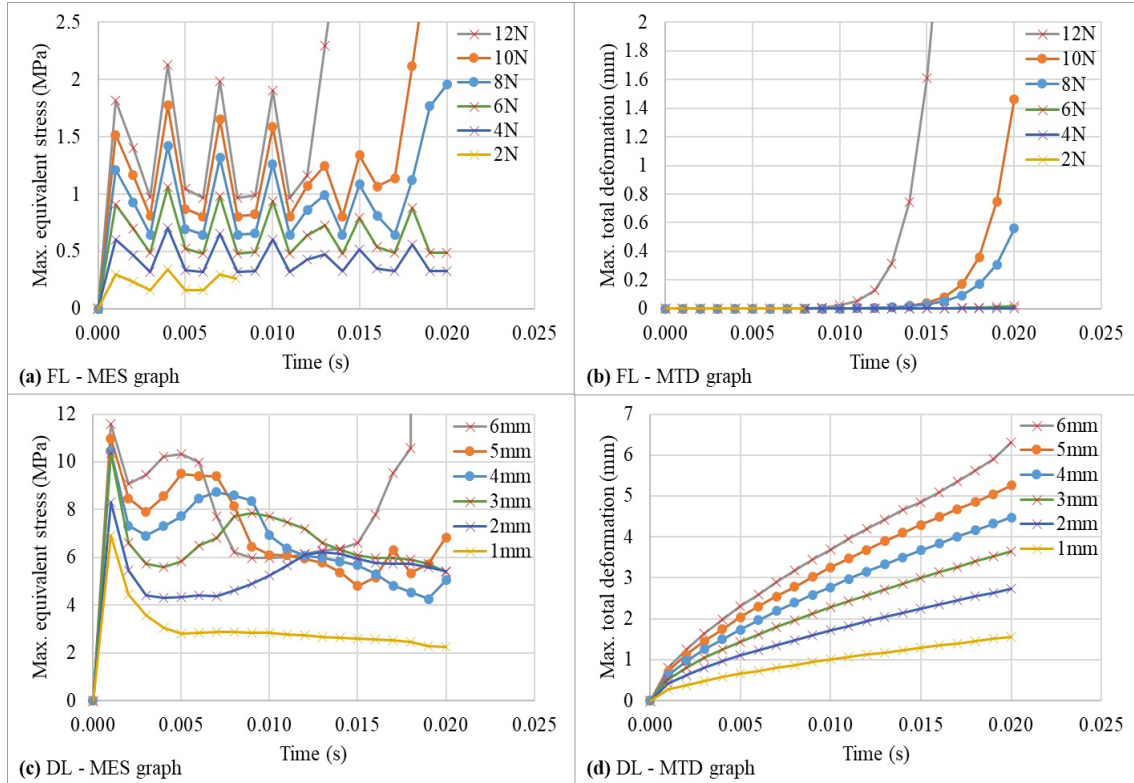


Figure 9. Results graphs obtained from numerical analysis

#### 4. CONCLUSION

In this study, the compressive strength test was numerically modeled in a computer environment according to the ASTM D695-15 standard. The effects of different force (2 N, 4 N, 6 N, 8 N, 10 N, 12 N) and different displacement (1 mm, 2 mm, 3 mm, 4 mm, 5 mm, 6 mm) loads applied in numerical analysis were investigated on the compressive strength of the test specimen. The results obtained from the study were listed below.

In the numerical analyses performed under different compression forces by defining FL, it was determined that;

- as the applied force increases, the stresses and total deformation on the test specimen also increase,
- in the analyses performed with 2 N, 4 N and 6 N compression forces, the test specimen did not suffer buckling damage,
- in the analyses performed with 8 N and 10 N compression forces, some buckling occurred,
- in the analysis performed with 12 N compression force, the test specimen was completely deformed,
- in the analysis performed with 4 N compression force, some compression deformation started in the middle region of the test specimen,
- in the analysis performed with 6 N compressive force, the compressive deformation in the middle region spread to the entire section,
- in the analysis performed with 8 N compression force, buckling started in the middle region,
- in the analyses performed with 8 N and 10 N compression forces, the highest total deformation occurred in the middle regions of the test specimen,
- in the analysis performed with 12 N compression force, the highest total deformation occurred in the upper part of the test specimen.

In the numerical analyses performed under different compression displacements by defining DL, it was determined that;

- as the applied displacement increases, the stresses and total deformation on the test specimen also increase,
- buckling damage occurred at all applied different compression displacements,
- as the amount of displacement increases, the amount of buckling also increases,
- in the analyses performed with 1 mm, 2 mm and 3 mm compression displacements, the highest total deformation occurred in the middle regions of the test specimen,
- in the analyses performed with 4 mm, 5 mm and 6 mm compression displacements, the highest total deformation occurred in the upper part of the test specimen.

## 5. REFERENCES

1. Dwivedi, K., Joshi, S., Nair, R., Sapre, M.S. & Jatti, V. (2024). Optimizing 3D printed diamond lattice structure and investigating the influence of process parameters on their mechanical integrity using nature-inspired machine learning algorithms. *Materials Today Communications*, 38(108233), 1-15.
2. Vidakis, N., Petousis, M., Karapidakis, E., Mountakis, N., David, C. & Sagris, D. (2023). Energy consumption versus strength in MEX 3D printing of polylactic acid. *Advances in Industrial and Manufacturing Engineering*, 6(100119), 1-19.
3. Cláudio, R.A., Dupont, J., Baptista, R., Leite, M. & Reis, L. (2022). Behaviour evaluation of 3D printed polylactic acid under compression. *Journal of Materials Research and Technology*, 21, 4052-4066.
4. Johri, N., Agarwal, G., Mishra, R.K. & Thakur, H.C. (2022). FEM analysis of polymeric hybrid composites. *Materials Today: Proceedings*, 57, 383-390.
5. Pernet, B., Nagel, J.K. & Zhang, H. (2022). Compressive strength assessment of 3D printing infill patterns. *Procedia CIRP*, 105, 682-687.
6. Selvamani, S.K., Ngui, W.K., Rajan, K., Samykan, M., Kumar R.R. & Badadhe, A.M. (2022). Investigation of bending and compression properties on PLA-brass composite using FDM. *Physics and Chemistry of the Earth*, 128(103251), 1-8.
7. Subramaniyan, M., Karuppan, S.P.P., Anand A.P. & Vasanthan A.P. (2022). Survey on compression property of sandwich 3D printed PLA components. *Materials Today: Proceedings*, 66, 955-961.
8. Srinivasan, T., Suresh, G., Ramu, P., Vignesh, R., Harshan, A.V. & Vignesh, K.P. (2021). Effect of hygrothermal ageing on the compressive behavior of glass fiber reinforced IPN composite pipes. *Materials Today: Proceedings*, 45, 1354-1359.
9. Morales, N.G., Fleck, T.J. & Rhoads, J.F. (2018). The effect of interlayer cooling on the mechanical properties of components printed via fused deposition. *Additive Manufacturing*, 24, 243-248.
10. Vidakis, N., Petousis, M., Vairis, A., Savvakis, K. & Maniadi, A. (2017). On the compressive behavior of an FDM Steward Platform part. *Journal of Computational Design and Engineering*, 4(4), 339-346.
11. Cocchi, A., Montagnier, O. & Hochard, C. (2021). Study of hourglass-shaped specimens for the analysis of compression behaviour in fibre direction of FRP composites using compression and four-point bending tests. *Composites Part A: Applied Science and Manufacturing*, 144(106332), 1-12.
12. Haseebuddin, M.R., Santhosh, S. & Shandilya, A.B. (2021). Development and characterization of PET flakes reinforced polyester resin composites. *Materials Today: Proceedings*, 46, 6075-6082.
13. Squires, C.A., Netting, K.H. & Chambers, A.R. (2007). Understanding the factors affecting the compressive testing of unidirectional carbon fibre composites. *Composites Part B: Engineering*, 38(4), 481-487.
14. ASTM D695 – 15, (2015). Standard test method for compressive properties of rigid plastics. *ASTM International*, <https://doi.org/10.1520/D0695-15>. Date of access: 31.03.2022.
15. Product Information Compression test kits (end-loading), (2024). *Zwick Roell*, [https://www.zwickroell.com/fileadmin/content/Files/SharePoint/user\\_upload/PI\\_EN/10\\_807\\_Compression\\_test\\_kits\\_end\\_loading\\_PI\\_EN.pdf](https://www.zwickroell.com/fileadmin/content/Files/SharePoint/user_upload/PI_EN/10_807_Compression_test_kits_end_loading_PI_EN.pdf). Date of access: 17.10.2024.

